Effect of Solvent Choice on the Self-Assembly Properties of a Diphenylalanine Amphiphile Stabilized by an Ion Pair

Enric Mayans,[a, b] Gema Ballano,[c] Javier Sendros,[a, b] MerÅH Font-Bardia,[d, e] J. Lourdes Campos,[a], Jordi Puiggal[&,*[a, b]], Carlos Cativiela,[*[c]] and Carlos Alem#n[*[a, b]]

[a] E. Mayans, J. Sendros, Dr. J. L. Campos, Prof. Dr. J. Puiggal&, Prof. Dr. C. Alem#n
Departament d'Enginyeria Qu&mica Universitat PolitHcnica de Catalunya EEBE, Edifici I.2, C/ Eduard Maristany, 10–14, 08019 Barcelona (Spain)
E-mail: jordi.puiggali@upc.edu
carlos.aleman@upc.edu

[b] E. Mayans, J. Sendros, Prof. Dr. J. Puiggal&, Prof. Dr. C. Alem#n
Barcelona Research Center for Multiscale Science and Engineering Universitat PolitHcnica de Catalunya C/ Eduard Maristany, 10–14, 08019 Barcelona (Spain)
E-mail: jordi.puiggali@upc.edu
carlos.aleman@upc.edu

[c] Dr. G. Ballano, Prof. Dr. C. Cativiela
Department of Organic Chemistry and Instituto de S&ntesis Quimica y Catalisis Homogenea (ISQCH)
University of Zaragoza-CSIC 50009 Zaragoza (Spain)
E-mail: cativiela@unizar.es

[d] Dr. M. Font-Bardia
Departament de Mineralogia, Cristallografia i Depksits Minerals Universitat de Barcelona Facultat de Geologia, c/Mart& i FranquHs, 08028 Barcelona(Spain)

[e] Dr. M. Font-Bardia
Unitat de Difraccij de Raigs X, Centre Cient&fic y Tecnolkgic Universitat de Barcelona C/Sol8 i Sabar&s 1, 08028 Barcelona (Spain)

.

ABSTRACT:

A diphenylalanine (FF) amphiphile blocked at the C terminus with a benzyl ester (OBzl) and stabilized at the N terminus with a trifluoroacetate (TFA) anion was synthetized and characterized. Aggregation of peptide molecules was studied by considering a peptide solution in an organic solvent and adding pure water, a KCl solution, or another organic solvent as co-solvent. The choice of the organic solvent and co-solvent and the solvent/ co-solvent ratio allowed the mixture to be tuned by modulating the polarity, the ionic strength, and the peptide concentration. Differences in the properties of the media used to dissolve the peptides resulted in the formation of different self-assembled microstructures (e.g. fibers, branched-like structures, plates, and spherulites). Furthermore, crystals of TFA·FFOBzl were obtained from the aqueous peptide solutions for Xray diffraction analysis. The results revealed a hydrophilic core constituted by carboxylate (from TFA), ester, and amide groups, and the core was found to be surrounded by a hydrophobic crown with ten aromatic rings. This segregated organization explains the assemblies observed in the different solvent mixtures as a function of the environmental polarity, ionic strength, and peptide concentration.

1. INTRODUCTION

In their pioneering work, Reches and Gazit[1] demonstrated the formation of diphenylalanine (FF, for which F=l-Phe) nanotubes in aqueous solution; these nanotubes were formed due to the directionality offered by a combination of hydrogen bonding and repeated phenyl stacking interactions. In subsequent studies, FF was proven as a minimal sequence that formed self-assembled peptide nanostructures,[2–8] and this gave way to the development of a new class of biomaterials that are based on the addition of various N- and C-terminal capping groups to aromatic FF or that are based on chemical modification of the F residues.

The peptide amphiphile Fmoc-FF (Fmoc=9-fluorenylmethoxycarbonyl), which forms stable gels, is among the most studied FF-based biomaterials. Thus, Fmoc-FF gels with a variety of properties have been prepared by using different approaches.[9] Gazit and co-workers formed gels by dissolving Fmoc-FF in an appropriate water-miscible solvent,[10, 11] whereas Ulijn and co-workers used a pH-switch approach coupled with changes in the temperature to yield Fmoc-FF gels with variable properties (i.e. depending on the rate of decrease in the Ph and the final pH).[12–15] The mixing method was also used by other groups, and it was shown that the mechanical properties of Fmoc-FF gels depended on the final ratio of dimethyl sulfoxide (DMSO) to water.[16, 17] More recently, Adams and coworkers formed Fmoc-FF gels by dissolving the peptide in an organic solvent (OS) and adding water, and the rheological properties depended on the choice of the OS.[18] Furthermore, gels formed by using acetone were metastable and single crystals suitable for X-ray diffraction were collected. The structure showed parallel stacking of the Fmoc-FF molecules with the neighboring molecules interacting through hydrogen bonds and weak offset p–p interactions.[18] Similarly, studies on Nap-peptide, capped with Fmoc and 9-fluorenylmethyl ester (OFm) groups at the N and C terminals, respectively, exhibited a great variety of polymorphic microstructures (e.g. doughnut, stacked braids, dendritic, and microtubes) depending on the solvents used to promote the self-assembly.[20] Notably, stacking interactions play a dominant role in such highly aromatic peptides.

An alternative approach is the chemical modification of the F residues. Reches and Gazit[5] explored the self-assembly of FF-based dipeptides in which the phenyl side chains were modified by halogen atoms, additional phenyl groups, or nitro substitutions. These homoaromatic dipeptide motifs formed tubular, spherical, and fibrillary structures in the nanoscale, and in some cases, nanocrystals and 2D nanoplates were also detected. These results proved that the properties of FF-based biomaterials could be properly tailored by engineering the F residue.

Another investigated strategy is the co-assembly of FFbased biomaterials with other molecules bearing aromatic groups.[15, 21–23] This approach, which may provide intermolecular transfer mechanisms,[24, 25] was applied to the Npm-FF (Npm=naphthoxymethyl) donor/dansyl acceptor system.[21] Peptide fibers based partly on aromatic stacking interactions with the dansyl component intercalated within this structure exhibited a redshift in the fluorescence emission and corresponding quenching of the emission

associated with the donor species.[21] Besides, hydrogels derived from the co-assembly of Fmoc-FF and Fmoc-diglycine[22] (Fmoc-GG) or Fmoc- Arg-Gly-Asp (Fmoc-RGD)[15] showed higher elastic moduli than Fmoc-FF alone, whereas the combination of Fmoc-FF with Fmoc-Lys (Fmoc-K), Fmoc-Ser (Fmoc-S), or Fmoc-Asp (Fmoc-D) resulted in significant changes in the rheological properties and fiber morphology.[23]

Besides, solvent-induced structural transitions have been examined by different authors. Li and co-workers[26] reported the transition of an organogel obtained by self-assembly of FF in toluene into a lower-like microcrystal merely by introducing ethanol as a co-solvent. Huang et al.[27] reported the structural transition of self-assembled FF from microtubes into nanofibers by introducing acetonitrile as a co-solvent in the water phase. Kumaraswamy et al.[28] found that the dimensions of the FF nanotubes were strongly influenced not only by the temperature and pH but also by the ionic strength of the solution. Mba and co-workers[29] synthetized two organogelators based on a pyrene moiety linked to FF that formed spherical aggregates and entangled fibrillary networks in acetonitrile and o-dichlorobenzene, respectively. Wang et al.[30] used FF to prove that a trace amount of a solvent could be a predominant factor to tune the self-assembly of peptides. More specifically, these authors showed that the addition of very small amounts of solvents forced the formation of solvent-bridged hydrogen bonds, which was a crucial interaction in directing fiber formation.

In this paper, we use the solvent-mixing method (i.e. dissolving the peptide in an OS and adding water or another OS as a co-solvent) to examine the self-assembly of a new FF-based amphiphile. In this new compound, hereafter denoted TFA·FFOBzl (Scheme 1), the C terminus is capped with a benzyl ester OBzl) group and the protonated amino group is stabilized to form an ion pair with trifluoroacetate (TFA). Accordingly, the aromatic interactions are expected to be weaker than those in Fmoc-FF, Nap-FF, and Fmoc-FF-OFm, whereas the dominant role played by intermolecular electrostatic interactions in FF is expected to decrease considerably because of the stability provided by TFA.

.

2. RESULTS AND DISCUSSION

The results presented in this work correspond to the conditions under which repetitive, stable, and structured morphologies were observed. More specifically, assemblies were required to fulfill the following conditions: one, to present a clearly defined morphology; two, to be systematically observed if the same conditions are used in different and independent experiments; three, to remain formed upon manipulation for optical microscopy, scanning electron microscopy (SEM) and/or atomic force microscopy (AFM) observations.

2.1. Peptide Synthesis and Preparation of Initial TFA·FF-OBzl Solutions

The synthesis of TFA·FF-OBzl was performed by following the procedure provided in Figure 1.
As the main aim of this study was to investigate the influence of both the polarity of the medium and the peptide concentration in the assembly of TFA·FF-OBzl, a two-step proce-dure was used. First, concentrated (5.0 mgmL@1) stock solutions were prepared by using solvent able to dissolve the peptide completely. For this purpose, four solvents with very different polarities were selected: hexafluoroisopropanol (HFIP), dimethylformamide (DMF), DMSO, and Milli-Q water. The dielectric constants of such solvents are: e=16.7 (HFIP), 37.2 (DMF), 46.7 (DMSO), and 78.5 (water). Second, the peptide concentration and the polarity of the medium were altered by direct addition of a co-solvent to the stock solution. In addition to the abovementioned solvents, both methanol (MeOH, e=32.6) and chloroform (CHCl3, e=4.7), which are not able to dissolve the peptide completely, were considered as co-solvents. This procedure allowed the peptide concentration to be varied in the prepared solvent/co-solvent mixtures between 0.05 and 4.8 mgmL@1. Both the final peptide concentration and the chemical nature of the mixture will be provided for each discussed structure. For the formation of the assembled structures, 10 or 20 mL aliquots of the prepared peptide solutions were placed on microscope coverslips or glass slides (glass sample holders) and were kept at room temperature (21 8C) or inside a cold chamber (4 8C) until dryness. The humidity was kept constant in both laboratories at 50%. Notably, no thermal treatment was applied to improve the solubility of the peptide or to accelerate the evaporation of the solvents. In spite of the huge number of conditions examined, the structures obtained under all of the conditions were carefully examined by optical microscopy. However, only those structures that fulfilled the requirements described above (i.e. well-defined morphology and reproducibility) were subsequently studied by SEM and AFM for discussion in this work.

2.2. Aqueous Environment

Dissolution of TFA·FF-OBzl into 2.0 mgmL@1 HFIP/water (4:6) directed the self-assembly process towards peptide nanofibers with a diameter (f) of about 250 nm, and these nanofibers align and pack to form well-defined microfibers that have diameters up to roughly 10 mm (Figure 2a). At the same time, such microfibers form very dense aggregates with a spike-like morphology. As the polarity of the

mixture increases and the peptide concentration decreases in 0.1 mgmL@1 HFIP/water (1:49), the density of the aggregated microfibers decreases, whereas a very porous mesh of randomly oriented (bundled) fibers coexists that partially coats the spike-like supramolecular structure (Figure 2b). These bundled fibers exhibit very different diameters (i.e. from &100 nm to &1 mm) and do not present any kind of imperfection, as observed in the corresponding SEM and AFM images. The mesh is replaced by small needlelike crystals emerging from the spike-like microstructures in 1.0 mgmL@1 DMF/water (1:4) peptide solutions (Figure 2c). However, a remarkable difference is that such spikes are not formed by long aligned nanofibers, as observed in Figure 2a for the 2.0 mgmL@1 HFIP/water (4:6) mixture, but by relatively short and sometimes broken interconnected nanofibers. These results suggest that the structure of the nanofibers, as well as their supramolecular organization (i.e. hierarchical self-assembly of TFA·FF-OBzl), change with both the polarity of the solvent mixture and the concentration of the peptide.

The addition of dilute KCl aqueous solutions (50 mm) to the HFIP, DMF, and DMSO peptide solutions causes drastic morphological changes, which mainly consist in the apparition of branched-like structures and, in some cases, ultrathin plates. Thus, poorly defined micrometric branched-like architectures (Figure 3a), which coexist with peptide microfibers (Figure S1 a, the Supporting Information), grow from 4.8 mgmL@1 HFIP/50 mm KCl (24:1) peptide solutions. However, microfibers coated with salt and with abundant defects (Figure S1 b) are the only structures observed upon reducing the peptide concentration to 1.0 mgmL@1. Furthermore, branched-like structures (Figure 3b), coexisting with disordered microfiber agglomerates (Figure S2), are obtained in 1.0 mgmL@1 DMF/50 mm KCl (1:4). The branching is more defined than that in Figure 3a, which suggests that this class of architecture can be promoted by enhancing both the polarity of the mixture and the ionic force.

The large influence of polarity is corroborated in Figure 3c for the 4.8 mgmL@1 DMSO/50 mm KCl (24:1) peptide mixture. In this case, well-defined branched structures, each one nucleating from a spherulite and partially coated with cubic crystals of salt, are abundantly detected. Both the central spherulite and the branches are made of ultrathin plates that, despite resembling lamellar crystal structures, are obtained through the hierarchical assembly of nanowires. If the peptide concentration decreases to 2.0 mgmL@1 and, consequently, the polarity and ionic strength of the DMSO/50 mm KCl (4:6) mixture increase, branches become poorly defined and less abundant (Figure S3), even though the self-assembly characteristics are similar to those described above for the concentrated peptide solution. Moreover, these supramolecular structures coexist with randomly distributed micrometric crystals that are oval in shape (Figure 3d). Finally, if the peptide concentration is reduced, for example, in 0.25 mgmL@1 DMSO/50 mm KCl (1:19),spherulitic-like microstructures surrounded by large salt crystals are observed (Figure 3e). According to the micrographs displayed in Figures 3c–e and S3, the combination of a polar OS (i.e. e=46.2 for DMSO) with an aqueous salt solution, KCl(aq), results in hierarchical assembly of the amphiphilic peptide under study, even though this tendency becomes less pronounced with decreasing amounts of DMSO (i.e. higher ionic strength). This feature should be

193 associated with the influence of solvent molecules and salt ions on the balance between peptide–peptide
194 and peptide–solvent interactions. The formation of branched-like structures is also considerably affected
195 by the pH. This is reflected in Figure S4, in which the pH of the corresponding OS/50 mm KCl solutions
196 was fixed at 10.5 by adding 0.5m NaOH. The poorly defined branched structures mentioned above for
197 the 4.8 mgmL@1 HFIP/50 mm KCl (24:1) mixture (Figure 2a) result in well-defined tree-like structures
198 of a fibrous nature at basic pH values (Figure S4 a). In contrast, the addition of NaOH transforms the
199 spherulite-nucleated branches observed in Figure 2c into dense bundles of plates that are irregularly
200 arranged (Figure S4 b). Indeed, some of these plates resemble deformed microtubes because of their
201 dimensions. This is reflected by the AFM cross-sectional profile displayed in Figure S4 b, which shows
202 that the x and y diameters for one such element are around 2.3 and 2.0 mm, respectively. These changes
203 are attributed to neutralization of the peptide by NaOH. Thus, strong and nonspecific (nondirectional)
204 electrostatic interactions associated with the charged end groups are probably replaced by weak and
205 specific (directional) hydrogen bonds after neutralization, and these hydrogen bonds affect the definition
206 of the assemblies their growing.
207 Notably, the branch- and tree-like structures obtained for TFA·FF-OBzl do not resemble the dendritic
208 structures identified for FF[31] and Fmoc-FFFF-Fmoc.[20] Kim and co-workers[31] obtained highly
209 ordered multidimensional dendritic nanoarchitectures by self-assembling FF from an acidic buffer
210 solution. More recently, stable dendritic structures made of branches growing from nucleated primary
211 frameworks were observed for Fmoc-FFFF-OFm.[20] The fractal dimension of the FF and Fmoc-FFFF-
212 OFm dendrimers was determined to be 1.7, which evidences self-similarity and two-dimensional
213 diffusion-controlled growth.[20, 31] However, the branched and tree-like structures displayed in Figures
214 3 and S4a do not exhibit a primary nucleating framework or a repetitive pattern for growth of the
215 branches, which are essential to obtain the characteristic selfsimilarity of dendritic structures.
216
217 **2.3. Single Crystal X-ray Structure of TFA·FF-OBzl**
218 The X-ray diffractograms were collected for prism-like crystals obtained by slow evaporation of a 0.415
219 mgmL@1 solution of TFA·FF-OBzl in Milli-Q water at 808C. Table S1 summarizes the main
220 crystallographic data of TFA·FF-OBzl, whereas Table S2 shows the final atomic parameters (fractional
221 coordinates and thermal factors) together with the estimated standard deviations. Geometric parameters
222 are listed in Tables S3 (bond lengths and angles) and Table S4 (torsional angles).
223 The conformation of a single TFA·FF-OBzl molecule is shown in Figure 4a together with labeling of
224 atoms and the corresponding displacement ellipsoids. It is clear that the molecule adopts a folded
225 conformation, and the peptide group is practically planar (C10@N1@C1@C2 @173.38) with f
226 (C1@N1@C10@ C11) and y (N2@C2@C1@N1/N1@C10@C11@O3) torsional angles of @86.6 and
227 127.7/@54.98, respectively. Notably, such a conformation does not fit to that expected for a
228 conventional b strand within a b sheet, which typically exhibits f and y values around @135 and +1358.
229 This feature is attributed to the formation of an intramolecular p–p stacking interaction between the

C13@C18 benzyl (Bzl) and C20@C25 phenyl (Ph) rings, which is indicated by a red arrow in Figure 4a. The dihedral angle between the Bzl and Ph aromatic groups is 33.68, whereas the distance between the centroids of the two rings is 4.59 a.

TFA·FF-OBzl crystallizes in an orthorhombic unit cell containing four molecules (Figure S5) that are related by binary screw axes, as is typical of chiral organic molecules. Figure 4b depicts a scheme of the molecular packing (b–c projection) with two neighboring molecules. The existence of a hydrophilic core, which is formed by the carboxylate (from TFA), ester, and amide groups, is particularly noticeable. This hydrophilic core is surrounded by a hydrophobic crown (dashed circle) formed by ten aromatic rings (i.e. six phenyl rings and four benzyl rings). Only six of these rings belong to the two represented molecules, whereas the other four are associated to neighboring ones. Table S5 summarizes the hydrogen-bonding interactions that can be considered and that involve ester, amide, and carboxylate groups. The most relevant intermolecular hydrogen bond, which is formed along the a direction, involves the N@H (amide) and C=O (ester) groups of molecules with a parallel orientation, as displayed in Figure 4c. It is remarkable that the C=O bond of the amide group only forms a weak interaction with terminal NH3 + groups. Finally, intermolecular p–p stacking interactions involving the C4@C9(Ph)···C13@C18(Bzl) and C4@C9(Ph)···C20@C25(Ph) aromatic rings are also present, and the distance between the centroids is around 4.5 a.

Peptide···peptide intermolecular electrostatic, hydrogen bonds, and p–p stacking interactions are known to be essential contributors to the formation of FF nano- and microarchitectures.[32] According to its crystal structure, the importance of these intermolecular forces is maintained in the assembly of the TFA·FF-OBzl amphiphile. Thus, on the basis of the morphology of the assembled structures and on the positions of the molecules in the crystal structure reported in this work, as the solvent gradually evaporates, the individual TFA·FF-OBzl molecules tend to form intermolecular electrostatic and p–p stacking interactions, which promotes the aggregation of peptide molecules and the formation of amphiphile crowns. The formation of a hydrophobic crown in the aggregates is reinforced by intramolecular p–p stacking interactions. These interactions result in the formation of b-sheet structures, which stack vertically through hydrogen bonds, and this results in lengthening of the peptide structure. This process is similar to that reported for amyloid fibril formation, even though in that case aggregates were usually formed through electrostatic and hydrogen-bonding interactions (i.e. p–p stacking interactions frequently participate in lengthening of the structure).[33]

2.4. Organic Environment

Dissolution of the peptide in a single OS resulted in a turbid solution with white particles (flocs) in suspension, and the combination of two OSs was necessary to obtain clear solutions and the subsequent self-assembly processes. Different levels of organization were obtained depending on the polarity of the mixture. Results are summarized in Figure 5.

Concentrated peptide solutions (+4 mgmL@1) in polar organic mixtures, such as DMF/MeOH, result in well-defined microfibers (f ranging from 2.5 to 5.5 mm) with a smooth surface (Figure 5a), and these microfibers tend to adopt a preferential alignment, crossed perpendicularly by fibers of smaller diameters (f&0.7–0.9 mm). Microfibers transform into microplates if the polarity of the environment decreases (+4 mgmL@1 HFIP/MeOH), whereas crossed sub-microfibers change their perpendicular orientation for a tilted one (&458). Thus, the most remarkable feature caused by reducing the polarity is the branched-like supramolecular organization of the peptide (Figure 5b). This feature becomes more pronounced in the leastpolar environment (4.0 mgmL@1 HFIP/CHCl3), in which spherulitic-like structures made of microplates are frequently identified (Figure 5c).

Notably, structures obtained at low peptide concentrations are disordered (i.e. without a well-defined morphology) and are poorly reproducible in all cases. As a hypothesis, this can be attributed to the fact that the organization of the amphiphilic molecules forming hydrophobic crowns is difficult in organic solvents, which evaporate faster than water. Thus, a high amount of peptide molecules are presumably required to form regular structures with well-defined morphologies, such as those displayed in Figure 5.

Overall, the results obtained in OSs indicate that the polarity of the environment regulates the 3D arrangement of the sheets formed by the TFA·FF-OBzl molecules, and it is this 3D arrangement that controls the formation of tubes or plates. On the other hand, comparison of the supramolecular organizations observed in aqueous solutions and OSs reflects two general trends that are characteristic of the latter environment. First, the concentration of the peptide required to obtain a well-defined self-assembly process in organic environments is significantly higher (+4 mgmL@1) than that in aqueous solvents. Thus, in organic environments peptide–solvent interactions are energetically favored over peptide–peptide interactions. This suggests that in water-containing solutions (i.e. those with higher polarity), attractive interactions between polar groups and water are far from compensating the repulsive interactions between the solvent and the aromatic groups of the peptide. Second, the density of supramolecular structures is considerably higher in water-containing environments than in OSs, which corroborates our previous hypothesis. Thus, the interaction of the peptide with the organic solvent is less repulsive than the interaction of the peptide with water, which hinders the self-assembly process in the former environment.

2.5. Influence of the Surrounding Environment in the Assembly Mechanism

The single-crystal structure of TFA·FF-Bzl, which was obtained by slow evaporation from a pure water solution, evidences the construction of a network of hydrogen bonds formed by parallel strands, which also interact through intra- and intermolecular stacking interactions (Figure 4). Although the parallel disposition of the molecules is in agreement with that observed by Adams and co-workers for single crystals of Fmoc-FF collected from gels formed in acetone,[18] important differences are detected between the two structures. These differences correspond to the drastic separation between the hydrophilic and hydrophobic groups in TFA·FF-OBzl. Thus, TFA·FF-OBzl exhibits a hydrophobic

303 crown surrounding a hydrophilic core that contains all of the polar groups, whereas this separation is
304 much less pronounced in Fmoc-FF because of steric hindrance induced by the bulky Fmoc groups.[18]
305 The clear separation between the polar groups and the hydrophobic rings in TFA·FFOBzl facilitates
306 understanding of the influence of the solvent on the morphology of the self-assembled aggregates. Thus,
307 the crystal structure of TFA·FF-OBzl is considered representative to understand the behavior of
308 amphiphilic FF-based biomaterials in different environments.
309 The obtainment of peptide nano- and microfibers in OS/ water environments with low and very low
310 peptide concentrations (i.e. mixtures in which the high dielectric constant of water plays a dominant role
311 because of its high volume ratio with respect to the OS) is attributed to an assembly in which
312 hydrophobic and polar forces are equally important in promoting the longitudinal growth of the fiber,
313 whereas the interactions between the fiber surface and both the environment and the glass support are
314 stabilized by polar forces. Accordingly, the length of the fiber increases because of favorable
315 hydrophobic–hydrophobic and polar–polar interactions between regions with identical natures, whereas
316 polar groups remain exposed at the surface of the fibers (Figure 6a). Moreover, this simple model
317 explains that, for a given OS, the density of aggregated fibers decreases if the volume ratio of water as a
318 cosolvent increases (i.e. the polarity of the mixture increases). Thus, the favorable interactions between
319 the peptide polar groups and water molecules compensate the affinity between the surface polar groups
320 of the different fibers if the concentration of water in the solvents mixture is high enough.
321 An enhancement in the ionic strength of the OS/water peptide solution, which is achieved by replacing
322 Milli-Q water with a 50 mm KCl aqueous solution as an added co-solvent, results in the formation of
323 microstructures with branched-like architectures coexisting with continuous (nonbranched) fibers. The
324 observation of cubic KCl crystals and a reduction in continuous fibers with increasing ionic strength are
325 both consistent with the mechanism displayed in Figure 6b. Accordingly, the salt nanocrystals coating
326 the surface of the peptide fibers nucleate the branches that grow through favorable KCl···TFA·FF-OBzl
327 electrostatic interactions. The frequency of this branching process increases with the ionic strength of
328 the mixture, which explains the fact that the definition of the branched-like architectures and the
329 presence of nonbranched fibers decrease with increasing volume ratios of KCl aqueous solution in the
330 OS/cosolvent mixture.
331 Microstructures derived from the combination of two Oss also depend on the polarity of the mixture.
332 Polar environments with high peptide concentrations result in the formation of microfibers by a
333 mechanism similar to that displayed in Figure 6a, and they transform into microplates if the polarity of
334 the environment decreases. To reduce access of the hydrophilic core to the surface, a mechanism such as
335 that depicted in Figure 6c is proposed. In this mechanism, the 2D growth of the microstructure and the
336 predominant hydrophobic region at the boundary favor the formation of peptide–solvent interactions.
337 Moreover, as the polarity of the environment is not drastically low, the apparition of irregularities and
338 defects with the hydrophilic core exposed to the solvent does not represent a severe thermodynamic
339 penalty for generation of the microstructure. At high peptide concentrations, the affinity between the

hydrophobic surface regions provokes aggregation of the plates, as is displayed in Figure 6d, which gives place to spherulites.

Overall, the results displayed in this work in combination with the straightforward models schematized in Figure 6 provide a simple rationale that explains the assembly behavior of the TFA·FF-OBzl amphiphile. Accordingly, the morphology of microstructures derived from this peptide can be easily regulated by controlling both the solvent and the peptide concentration. This versatility makes TFA·FF-OBzl a very interesting system for applications that are mainly based on interactions with other chemical species, for example, drugs. Within this context, TFA·FF-OBzl microstructures are potential candidates to upload either polar or nonpolar drugs at their surface and, therefore, are potential candidates be used as versatile carriers and/or delivery systems. Thus, although some peptide amphiphiles have been previously suggested for delivery,[34, 35] their utility is typically restricted to the loading of polar or nonpolar drugs. However, the adaptability of TFA·FF-OBzl eliminates the restrictions related to the chemical nature of the used drugs, which gives a new dimension to this application.

3. CONCLUSIONS

We evidenced the remarkable control exerted by the characteristics of solvent mixtures on the organization of TFA·FF-OBzl (TFA=trifluoroacetate, FF=diphenylalanine, OBzl=benzyl ester) assemblies derived from the addition of a co-solvent to a peptide solution. Thus, the polarity, ionic strength, and peptide concentration in the mixture were regulated by adding a selected amount of a given co-solvent [i.e. pure water, 50 mm aq. KCl, or an organic solvent (OS)] to a concentrated peptide solution in hexafluoroisopropanol (HFIP), DMF, DMSO, or water. Although polar aqueous environments tended to promote the growth of fibers, which were found to co-exist with branched-like microstructures if Milli-Q water was replaced by 50 mm KCl, nonpolar environments obtained by mixing two OSs preferred peptide assemblies organized in plates and spherulites.

The X-ray diffractograms collected for single crystals of TFA·FF-OBzl revealed a segregated distribution of the hydrophilic and hydrophobic regions. More specifically, the carboxylate (from TFA), amide, and ester (both from FF-OBzl) groups were separated from a highly polar core stabilized through hydrogen- bonding interactions, and this core was found to be ringed by a hydrophobic crown involving ten aromatic rings. This unique organization enabled us to explain the influence of the solvent mixture properties on peptide assembly. Thus, growth of the peptide structure and exposure of the hydrophilic or hydrophobic region were simply determined by the formation of favorable peptide–solvent interactions at the surface.

Tuning the structure of TFA·FF-OBzl by changing the solvents used in the mixture is a very attractive feature to expand the potential utility of peptide assemblies in different fields, for example, as molecular carriers and delivery systems. Thus, both polar and nonpolar compounds could be easily loaded on TFA·FF-OBzl microstructures by regulating the assembly through the solvents used in the mixture.

EXPERIMENTAL SECTION

General Methods

Melting points were determined with a Gallenkamp apparatus and are uncorrected. IR spectra were registered with a Nicolet Avatar 360 FTIR spectrophotometer; the nmax values are given for the main absorption bands. 1H NMR and 13C NMR spectra were recorded with a Bruker AV-400 or ARX-300 instrument at room temperature by using the residual solvent signal as the internal standard Chemical shifts (d) are expressed in ppm, and coupling constants (J) are expressed in Hertz. Optical rotations were measured with a JASCO P-1020 polarimeter. High-resolution mass spectra were obtained with a Bruker Microtof-Q spectrometer.

Peptide Synthesis and Characterization Boc-FF-OBzl (3): HOBt·xH2O (1.01 g, 6.6 mmol) was added to a solution of Boc-F-OH (1; 1.75 g, 6.6 mmol) in dichloromethane (15 mL) cooled to 0 8C in an ice bath, and this was followed by the addition of EDC·HCl (1.27 g, 6.6 mmol). The mixture was stirred for 15 min, and then a solution of H-F-OR 2 (6.0 mmol) [obtained by the addition of DIPEA (1.25 mL, 7.2 mmol) to the TFA salt of 2] in dichloromethane (5 mL) and additional DIPEA (1.15 mL, 6.6 mmol) were added. The mixture was stirred for 1 h at 0 8C and then at room temperature for 24 h. The mixture was washed with 5% aq. NaHCO3 (3V15 mL) and 5% aq. KHSO4 (3V15 mL). The organic phase was dried with anhydrous magnesium sulfate and evaporated to dryness. The resulting solid was suspended in a diethyl ether/n-hexane mixture and was filtered under reduced pressure to provide 3 as a white solid. Yield: 90%; m.p. 180–1818C; ½aA25 D = @17.7 (c=0.33 in methanol); 1H NMR (400 MHz, CDCl3): d=1.32 (s, 9H), 2.92–3.02 (m, 4H), 4.21–4.30 (m, 1H), 4.72–4.76 (m, 1H), 4.86 (br s, 1H), 5.02 (s, 2H), 6.20 (d, J=7.6 Hz, 1H), 6.81–6.83 (m 2H), 7.07–7.14 (m, 5H), 7.16–7.21 (m, 5H), 7.26–7.32 ppm (m, 3H); 13C NMR (100 MHz, CDCl3): d=28.36, 38.07, 38.43, 53.44, 55.82, 67.35, 80.32, 127.11, 127.19, 128.65, 128.67, 128.70, 128.74, 128.79, 129.41, 129.49, 135.14, 135.61, 136.62, 155.39, 170.85, 170.90 ppm; IR (KBr): n˜=3332, 1741, 1696, 1681 cm@1; HRMS (ESI): m/z: calcd for C30H34N2NaO5: 525.2360 [M+Na]+; found: 525.2375.

For tert-butoxycarbonyl (Boc) deprotection, a solution of the corresponding Boc-protected compound in dichloromethane was treated with trifluoroacetic acid (TFA-H; 15 equiv.), and the mixture was stirred at room temperature for 1 h. After evaporation of the solvent, the residue was suspended in a diethyl ether/n-hexane mixture and filtered under reduced pressure to provide the corresponding TFA salt as a white solid in quantitative yield.

TFA·FF-OBzl (4): According to the general Boc-deprotection procedure, TFA (2 mL) was added to a solution of 3 (2.0 mmol) in dichloromethane (20 mL) to provide corresponding TFA salt 4 (Figure S6) in quantitative yield. M.p. 290–292 8C (decomp.); a ½ A20 D = +18.2 (c=0.36 in acetic acid); 1H NMR (400 MHz, [D6]DMSO: d= 2.90 (dd, J=14.2 Hz, J=8.3 Hz, 1H), 3.02 (dd, J=13.9 Hz, J=8.1 Hz, 1H), 3.08–3.13 (m, 2H), 4.05–4.13 (m, 1H), 4.63–4.69 (m, 1H), 5.06– 5.14 (m, 2H), 7.22–7.38 (m, 15H), 8.23 (br s, 2H), 9.15 ppm (d, J= 7.5 Hz, 1H); 13C NMR (100 MHz, [D6]DMSO): d=36.79, 36.99, 53.21,

54.03, 66.37, 111.85, 114.77, 117.68, 120.60, 126.80, 127.19, 128.09, 128.20, 128.45, 128.54, 129.18, 129.59, 134.79, 135.60, 136.65, 158.05, 158.40, 158.75, 159.10, 168.43, 170.71 ppm; IR (KBr): n˜= 3342, 1725, 1695, 1662 cm@1; HRMS (ESI): m/z: calcd for C25H26N2NaO3: 425.1836 [M+Na]+; found: 425.1821.

Sample Preparation

Peptide-containing solutions (25 or 100 mL) were prepared from 5 mgmL@1 stock solutions by using HFIP, DMF, DMSO, and Milli-Q water as solvents. The peptide concentration was reduced by adding Milli-Q water, MeOH, or CHCl3 as co-solvent to a given stock solution. More specifically, peptide concentrations of 4.8, 4.0, 2.0, 1.0, 0.3, 0.25, and 0.1 mgmL@1 were obtained by using 24:1, 4:1, 4:6, 1:4, 3:47, 1:19, and 1:49 solvent/co-solvent ratios, respectively. On the other hand, the 50 mm aq. KCl solution was used as a co-solvent to modify the ionic strength. Finally, 10 or 20 mL aliquots were placed on microscope coverslips and kept at room temperature (25 8C) or inside a cold chamber (4 8C) until dryness. All organic solvents were purchased from Sigma–Aldrich, Fisher Scientific, and Scharlab.

Optical Microscopy

Morphological observations were performed by using a Zeiss Axioskop 40 microscope. Micrographs were taken with a Zeiss Axios-Cam MRC5 digital camera.

Scanning Electron Microscopy (SEM)

SEM studies were performed with a Focussed Ion Beam Zeiss Neon 40 scanning electron microscope operating at 5 kV and equipped with an EDX spectroscopy system. Samples were mounted on a double-sided adhesive carbon disc and were sputter coated with a thin layer of carbon to prevent sample charging problems.

Atomic Force Microscopy (AFM)

Topographic AFM images were obtained by using either a Dimension 3100 Nanoman AFM or a Multimode, both from Veeco (Nano- Scope IV controller), under ambient conditions in tapping mode. AFM measurements were performed on various parts of the morphologies, which produced reproducible images similar to those displayed in this work. Scan window sizes ranged from 5V5 to 80V80 mm2.

Crystallization and X-ray Diffraction

Colorless prism-like crystals (0.010 mm V 0.020 mm V 0.100 mm) were obtained by slow evaporation at 808C of a 0.415 mgmL@1 solution of TFA·FF-OBzl in MQ-grade water and were used for X-ray diffraction analysis. The X-ray intensity data were measured with a D8 Venture system equipped with a multilayer monochromator and a Cu microfocus (l=1.54178 a).

The frames were integrated with the Bruker SAINT software package by using a narrow-frame algorithm. Integration of the data using an orthorhombic unit cell yielded a total of 13671 reflections to a maximum q angle of 79.258 (0.78 a resolution), of which 5037 were independent (average redundancy 2.714, completeness= 95.0%, Rint=4.97%, Rsig=5.67%) and 4499 (89.32%) were greater than 2s(F2). The final cell constants of a=5.8856(3) a, b= 18.5677(9) a, c=23.0370(11) a, and volume=2517.5(2) a3 are based upon the refinement of the xyz centroids of reflections above 2q s(I). Data were corrected for absorption effects by using the multiscan method (SADABS). The calculated minimum and maximum transmission coefficients (based on crystal size) are 0.6156 and 0.7461.

The structure was solved and refined by using the Bruker SHELXTL software package by using the P212121 space group with Z=4 for the formula unit, C27H27F3N2O5. The final anisotropic full-matrix least-squares refinement on F2 with 335 variables converged at R1=4.26% for the observed data and wR2=14.04% for all data. The goodness-of-fit was 1.032. The largest peak in the final difference electron density synthesis was 0.289 ea@3, and the largest hole was @0.257 ea@3 with a root-mean square deviation of 0.059 ea@3. On the basis of the final model, the calculated density was 1.363 gcm@3 and F(000) was 1080 e.

ACKNOWLEDGEMENTS

The authors are thankful for support from MINECO and FEDER (MAT2015-69367-R, MAT2015-69547-R and CTQ2013-40855-R) and Gobierno de Aragjn—Fondo Social Europeo (research group E40). Support for the research of C.A. was received through the prize “ICREA Academia” for excellence in research funded by the Generalitat de Catalunya.

Keywords: fibers · hydrophilic core · nanostructures · peptide materials · stacking interactions

[1] M. Reches, E. Gazit, Science 2003, 300, 625–627. [2] P. Tamamis, L. Adler-Abramovich, M. Reches, K. Marshall, P. Sikorski, L. Serpell, E. Gazit, G. Archontis, Biophys. J. 2009, 96, 5020–5029.

[3] C. H. Gçrbitz, Chem. Commun. 2006, 2332–2334.

[4] L. Adler-Abramovich, M. Reches, V. L. Sedman, S. Allen, S. J. B. Tendler, E. Gazit, Langmuir 2006, 22, 1313–1320.

[5] M. Reches, E. Gazit, Phys. Biol. 2006, 3, S10–S19.

[6] M. Reches, E. Gazit, Nano Lett. 2004, 4, 581–585.

[7] E. Mayans, G. Ballano, J. Casanovas, A. D&az, A. P8rez-Madrigal, F. Estrany, J. Puiggal&, C. Cativiela, C. Alem#n, Chem. Eur. J. 2015, 21, 16895–16905.

[8] X. Yan, J. Li, H. Mçhwald, Adv. Mater. 2011, 23, 2796–2801.

[9] J. Raeburn, A. Zamith Cardoso, D. J. Adams, Chem. Soc. Rev. 2013, 42, 5143–5156.

[10] A. Mahler, M. Reches, M. Rechter, S. Cohen, E. Gazit, Adv. Mater. 2006, 18, 1365–1370.

[11] N. Amdursky, R. Orbach, E. Gazit, D. Huppert, J. Phys. Chem. C 2009, 113, 19500–19505.

[12] V. Jayawarna, M. Ali, T. A. Jowitt, A. F. Miller, A. Saiani, J. E. Gough, R. V. Ulijn, Adv. Mater. 2006, 18, 611–614.

[13] A. M. Smith, R. J. Williams, C. Tang, P. Coppo, R. F. Collins, M. L. Turner, A. Saiani, R. V. Ulijn, Adv. Mater. 2008, 20, 37–41.

[14] C. Tang, A. M. Smith, R. F. Collins, R. V. Ulijn, A. Saiani, Langmuir 2009, 25, 9447–9453.

[15] M. Zhou, A. M. Smith, A. K. Das, N. W. Hodson, R. F. Collins, R. V. Ulijn, J. E. Gough, Biomaterials 2009, 30, 2523–2530.

[16] J. Raeburn, G. Pont, L. Chen, Y. Cesbron, R. Levy, D. J. Adams, Soft Matter 2012, 8, 1168–1174.

[17] N. A. Dudukovic, C. F. Zukoski, Langmuir 2014, 30, 4493–4500.

[18] J. Raeburn, C. Mendoza-Cuenca, B. N. Cattoz, M. A. Little, A. E. Terry, A. Z. Cardoso, P. C. Griffiths, D. J. Adams, Soft Matter 2015, 11, 927–935.

[19] V. Jayawarna, A. Smith, J. E. Gough, R. V. Ulijn, Biochem. Soc. Trans. 2007, 35, 535–537.

[20] E. Mayans, G. Ballano, J. Casanovas, L. J. del Valle, M. M. P8rez-Madrigal, F. Estrany, A. I. Jim8nez, J. Puiggal&, C. Cativiela, C. Alem#n, Soft Matter 2016, 12, 5475–5488.

[21] P. W. J. M. Frederix, R. Kania, J. A. Wright, D. A. Lamprou, R. Ulijn, C. J. Pickett, N. T. Hunt, Dalton Trans. 2012, 41, 13112–13119.

[22] W. Helen, P. de Leonardis, R. V. Ulijn, J. Gough, N. Tirelli, Soft Matter 2011, 7, 1732–1740.

[23] V. Jayawarna, S. M. Richardson, A. R. Hirst, N. W. Hodson, A. Saiani, J. E. Gough, R. V. Ulijn, Acta Biomater. 2009, 5, 934–943.

[24] Y. Yamauchi, M. Yoshizawa, M. Fujita, J. Am. Chem. Soc. 2008, 130, 5832–5833.

[25] K. V. Rao, S. J. George, Chem. Eur. J. 2012, 18, 14286–14291.

[26] P. Zhu, X. Yan, S. Su, Y. Yang, J. Li, Chem. Eur. J. 2010, 16, 3176–3183.

[27] R. Huang, W. Qi, R. Su, J. Zhao, Z. He, Soft Matter 2011, 7, 6418–6421.

[28] P. Kumaraswamy, R. Lakshmanan, S. Sethuraman, U. M. Krishnan, Soft Matter 2011, 7, 2744–2754.

[29] S. Bartocci, I. Morbioli, M. Maggini, M. Mba, J. Pept. Sci. 2015, 21, 871 – 878.

[30] J. Wang, K. Liu, L. Yan, A. Wang, S. Bai, X. Yan, ACS Nano 2016, 10, 2138–2143.

[31] T. H. Han, J. K. Oh, G.-J. Lee, S. I. Pyun, S. O. Kim, Colloids Surf. B 2010, 79, 440–445.

[32] C. H. Gorbitz, Chem. Eur. J. 2001, 7, 5153–5159.

[33] X. Yan, P. Zhu, J. Li, Chem. Soc. Rev. 2010, 39, 1877–1890.

[34] V. Castelletto, J. E. McKendrick, I. W. Hamley, U. Olsson, C. Cenker, Langmuir 2010, 26, 11624–1162.

[35] S. T. Kumar, J. Meinhardt, A. K. Fuchs, T. Aumeller, J. Leppert, B. Bechele, U. Knepfer, R. Ramachandran, J. K. Yadav, E. Prell, I. Morgado, O. Ohlenschl-ger, U. Horn, T. Simmet, M. Gçrlach, M. F-ndrich, ACS Nano 2012, 8, 11042–11052.

533 **Legends to figures**

534

535 **Scheme 1.** Chemical structure of TFA·FF-OBzl.

536

537 **Figure. 1** Scheme for the reactions used to obtain TFA·FF-OBzl. Reagents and conditions: a) N-[3-
538 (dimethylamino)-propyl]-N'-ethylcarbodiimide (EDC), 1-hydroxybenzotriazole (HOBt), N,N-
539 diisopropylethylamine (DIPEA), CH2Cl2, 08C, 30 min, then RT, 24 h; b) TFA, CH2Cl2, RT, 1 h.

540

541 **Scheme 2**. Synthesis of 2-methoxy-6-oxo-1,4,5,6 tetrahydropyridin-3-carbonitriles 1a–d.

542

543 **Figure. 2** Representative SEM and AFM (height) images of the structures derived from TFA·FF-OBzl
544 solutions in a) 2.0 mgmL@1 HFIP/water (4:6) at 48C, b) 0.1 mgmL@1 HFIP/water (1:4) at room
545 temperature, and c) 1.0 mgmL@1 DMF/water (1:4) at room temperature. The shape and hierarchical
546 self-assembly change with the polarity of the solvent mixture and the peptide concentration. Red circles
547 in panel c indicate broken nanofibers. 7a.

548

549 **Figure. 3** Representative SEM and AFM (height) images of the branched structures obtained at room
550 temperature from TFA·FF-OBzl dissolved in a) 4.8 mgmL@1 HFIP/50 mm KCl (24:1), b) 1.0
551 mgmL@1 DMF/50 mm KCl (1:4), c) 4.8 mgmL@1 DMSO/50 mm KCl (24:1), d) 2.0 mgmL@1
552 DMSO/50 mm KCl (4:6), and e) 0.25 mgmL@1 DMSO/50 mm KCl (1:19).

553

554 **Figure. 4** a) Scheme of the TFA·FF-OBzl molecule with displacement ellipsoids drawn at the 50%
555 probability level. H atoms are drawn as circles with arbitrary radii. b) View along the c axis showing the
556 packing of two molecules related by a binary screw axis. Dashed circle points out the aromatic rings that
557 are disposed around the inner hydrophilic part. H atoms are omitted for clarity. c) Scheme showing the
558 intermolecular hydrogen bonds established between neighboring chains along the a axis.

559

560 **Figure. 5** Representative SEM and AFM (height) images of the structures obtained at room temperature
561 from TFA·FF-OBzl dissolved in a) 4.0 mgmL@1 DMF/MeOH, b) 4.0 mgmL@1 HFIP/MeOH, and c)
562 4.0 mgmL@1 HFIP/CHCl3. Fiber-like organizations evolve into plate-like organizations with
563 decreasing polarity of the medium. The dielectric constants of DMF, HFIP, MeOH, and CHCl3 are
564 e=37.2, 16.7, 32.6, and 4.7, respectively.

565

566 **Figure. 6** Schemes explaining the self-assembly and aggregation of TFA·FFOBzl under different
567 conditions considering the hydrophilic (blue) and hydrophobic (red) regions observed in the
568 corresponding X-ray structure (Figure 4): a) fibers, b) branched fibers, c) plates, and d) spherulites.

569

570 **SCHEME 1**

571

572

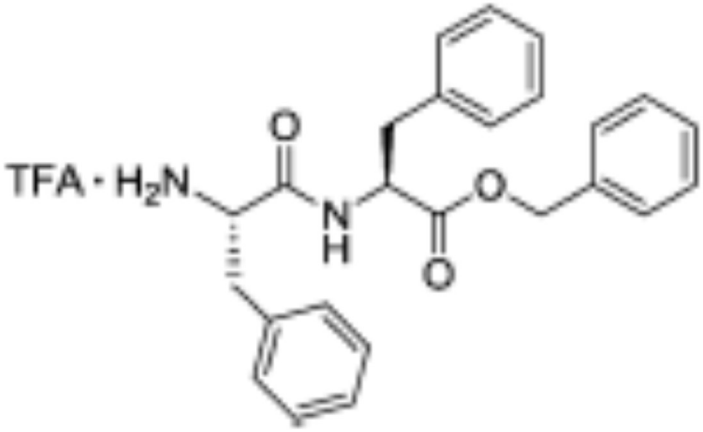

573

574

575

576

577
578 **FIGURE 1**

579

580

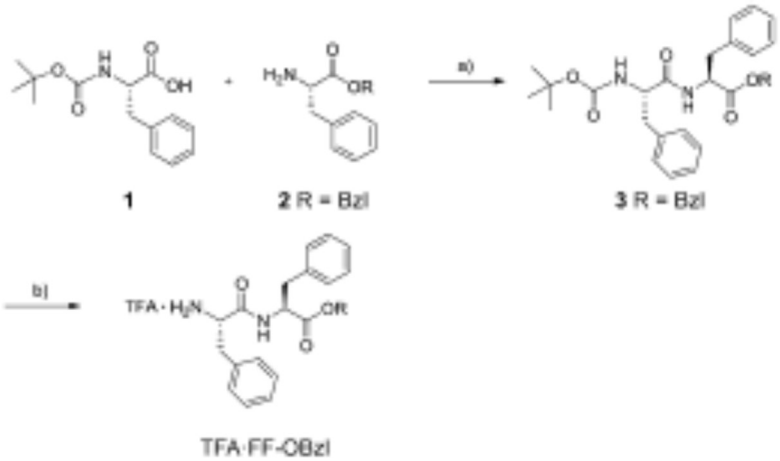

581

582

583

FIGURE 2

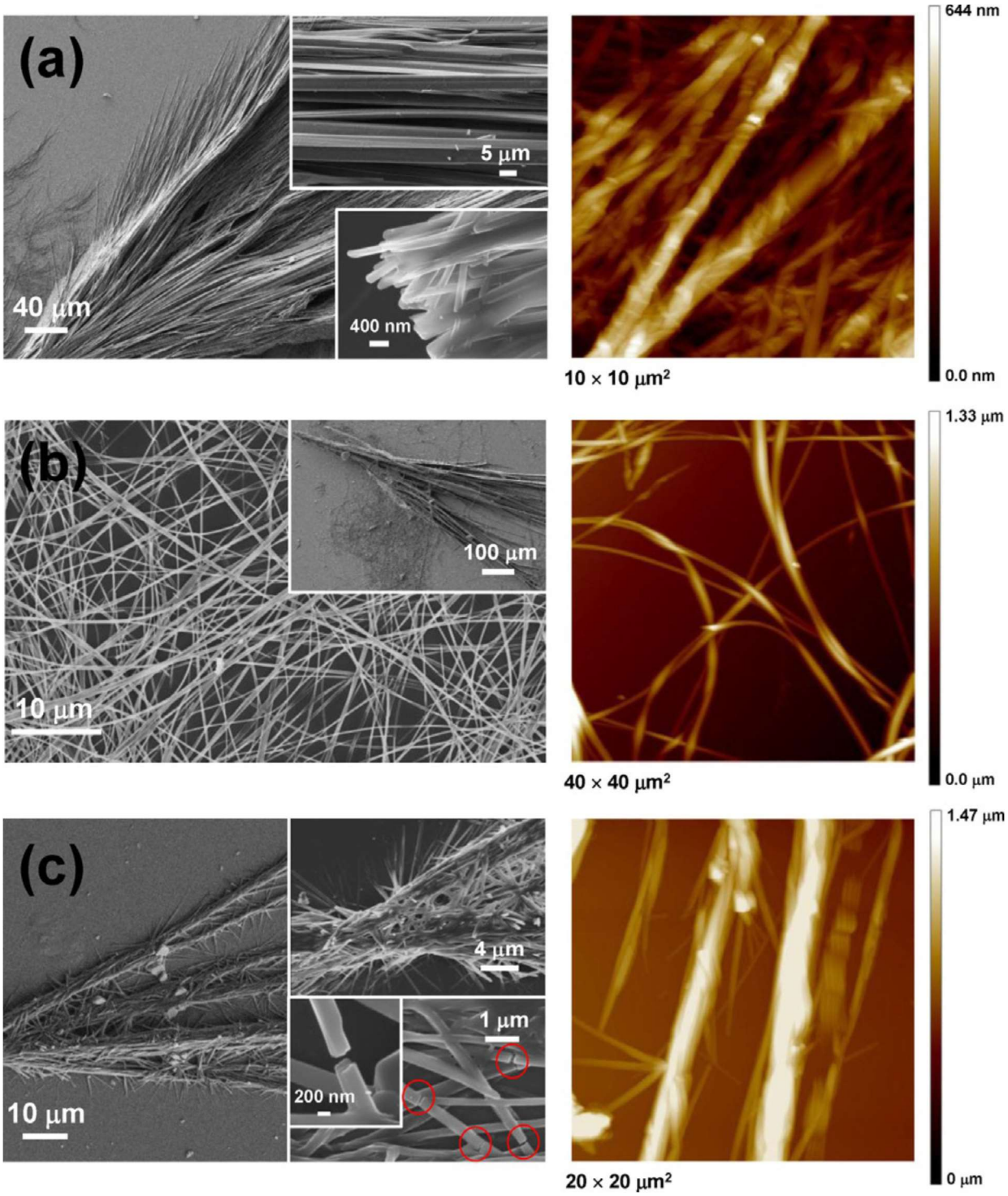
(a)
5 μm
40 μm
400 nm
10 × 10 μm²
644 nm
0.0 nm
(b)
100 μm
10 μm
40 × 40 μm²
1.33 μm
0.0 μm
(c)
4 μm
1 μm
200 nm
10 μm
20 × 20 μm²
1.47 μm
0 μm

591 **FIGURE 3**

592

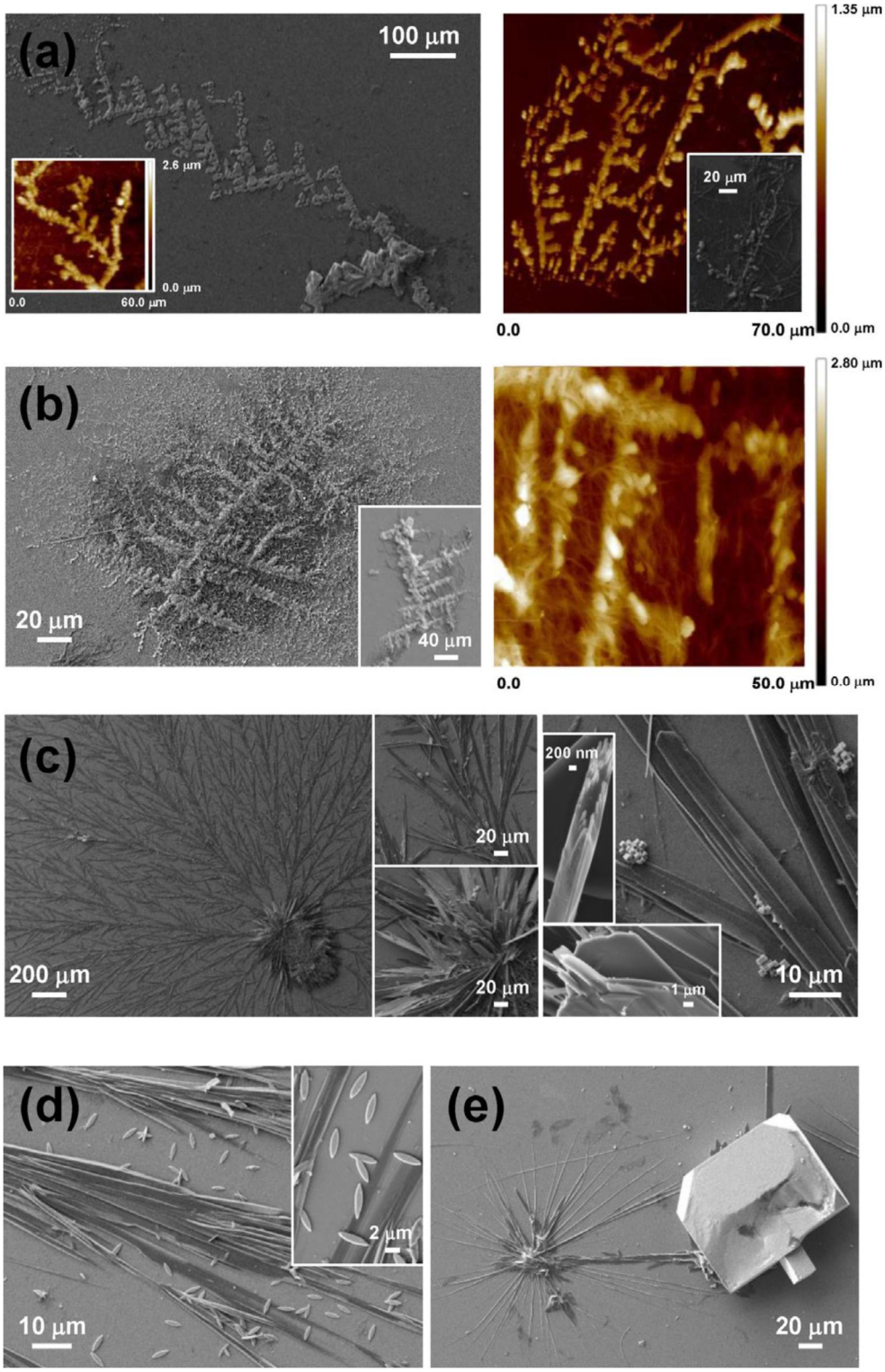

593

594

FIGURE 4

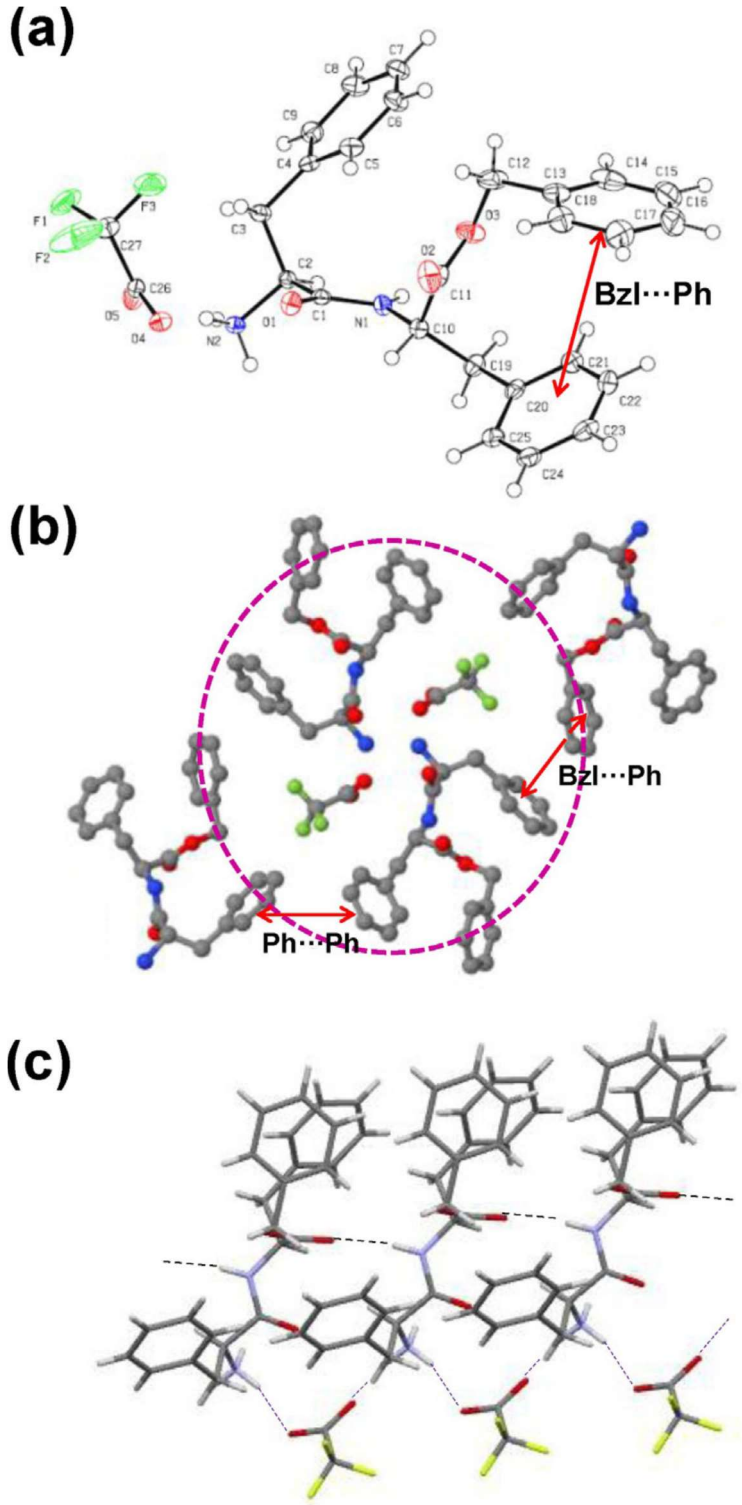

603 **FIGURE 5**

604

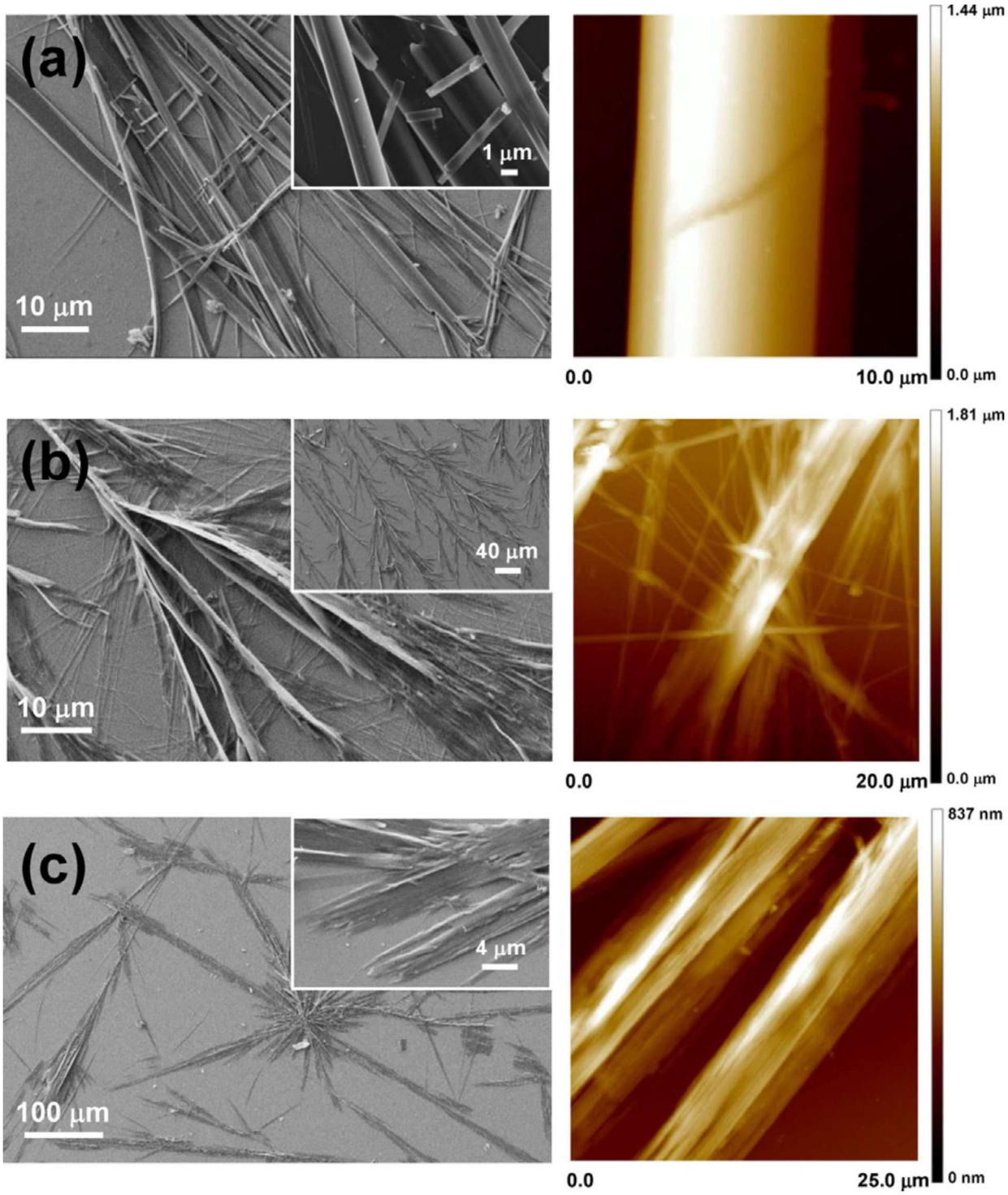

605

606

607

608

609

610 **FIGURE 6**

611

612

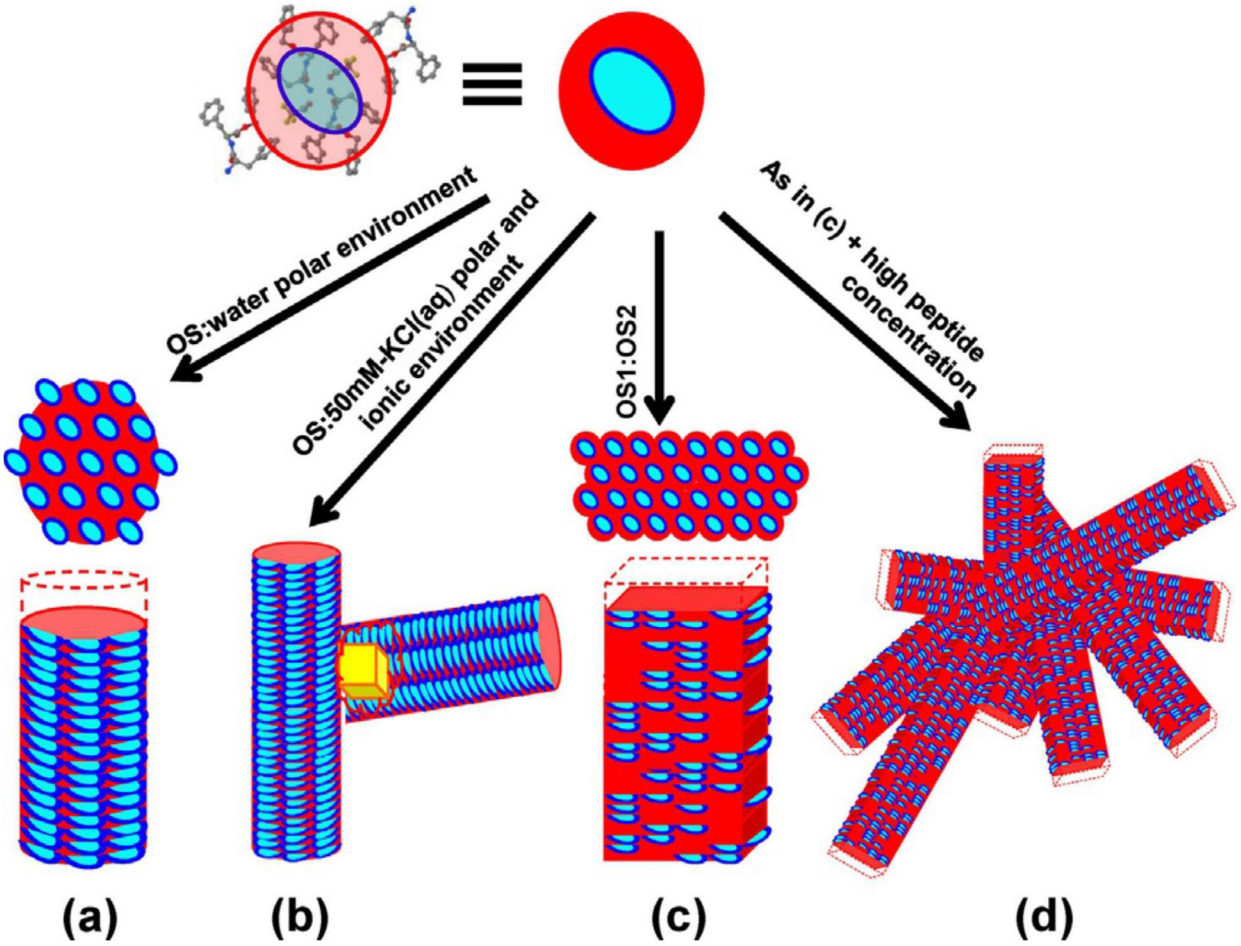

613